

# Long-term monitoring of Ark 120 with Swift

M. Gliozzi,<sup>1\*</sup> I.E. Papadakis,<sup>2,3</sup> D. Grupe,<sup>4</sup> W.P. Brinkmann,<sup>5</sup> and C. R  th<sup>6</sup>

<sup>1</sup> *Physics and Astronomy Department, George Mason University, 4400 University Drive, Fairfax, VA 22030*

<sup>2</sup> *Physics Department, University of Crete, 710 03 Heraklion, Crete, Greece*

<sup>3</sup> *Foundation for Research and Technology - Hellas, IESL, Voutes, 71110 Heraklion, Crete, Greece*

<sup>4</sup> *Department of Earth and Space Sciences, Morehead State University, Morehead, Kentucky, USA*

<sup>5</sup> *Max-Planck-Institut f  r extraterrestrische Physik, Postfach 1312, D-85741 Garching, Germany*

<sup>6</sup> *German Aerospace Center, Department of Complex Plasmas, K  ln, Germany*

5 April 2024

## ABSTRACT

We report the results of a six month *SWIFT* monitoring campaign of Ark 120, a prototypical “bare” Seyfert 1 galaxy. The lack of intrinsic absorption combined with the nearly contemporaneous coverage of the UV, and X-ray bands makes it possible to investigate the link between the accretion disk and the putative Comptonization corona. Our observations confirm the presence of substantial temporal variability, with the X-ray characterized by large-amplitude flux changes on timescales of few days, while the variations in the UV bands are smoother and occur on timescales of several weeks. The source also shows spectral variability with the X-ray spectrum steepening when the source is brighter. We do not detect any correlation between the UV flux and the X-ray spectral slope. A cross correlation analysis suggests positive delays between X-rays and the UV emission, favoring a scenario of disk reprocessing. Although the strength of the correlation is moderate with a delay that is not well constrained ( $7.5 \pm 7$  days), it is nevertheless indicative of a very large disk reprocessing region, with a separation between the X-ray and the UV emitting regions which could be as large as  $1000 r_G$ . The Ark 120 correlation results are in agreement with those obtained in similar multi-wavelength monitoring studies of AGN. When combined together, the observations so far can be well described by a linear relation between the X-ray/UV delays and the mass of the central black hole. Within the context of the simplest scenario where these delays correspond to light-travel times, the implied distance between the X-ray source and the optical/UV disk reprocessing region in these AGN should be of the order of many hundreds of gravitational radii.

**Key words:** Galaxies: active – Galaxies: nuclei – X-rays: galaxies

## 1 INTRODUCTION

Numerous observational studies across the electromagnetic spectrum have shown that active galactic nuclei (AGN) are powerful emitters of variable radiation from the radio band to  $\gamma$ -ray energies and that a sizable amount of this radiation is emitted in the optical, UV, X-ray energy bands. It is generally thought that AGN are powered by accretion onto a central supermassive black hole and that the optical-UV emission is the thermal radiation produced directly from the accretion flow, whereas the X-rays are produced through the Comptonization process in a putative corona. While this general picture is widely accepted, the details of the interaction between disk and corona, the geometry and physical

state of the latter, as well as the origin of the variability are still poorly understood.

One of the most promising approaches to shed some light on the inner region of black holes systems is to track the variable behavior of the different components of the central engine using multi-wavelength monitoring observations. Over the years, coordinated optical and X-ray monitoring observations of AGN have revealed that, in addition to the ubiquitous X-ray variability, long-term optical variations are consistently detected. The latter are generally interpreted as intrinsic variations of the disk emission caused by disturbances propagating across the disk or, alternatively, as a result of the disk reprocessing of the X-ray emission produced by the corona. In this context, various monitoring studies have yielded contrasting results, with some sources showing highly correlated optical/X-ray behavior with one band leading the other, and some others showing no correlation at

\* E-mail: mgliozzi@gmu.edu

all (e.g., Maoz et al. 2000; Uttley et al. 2003; Arévalo et al. 2009; Breedt et al. 2009; Arévalo et al. 2009; Breedt et al. 2010). Some of the inferred discrepancies may be attributed to the intrinsic difficulties of coordinating satellite-based X-ray monitoring with ground-based optical observations, which may also be hampered by weather conditions.

An important step forward in this field has been the advent of *SWIFT*, which, thanks to its flexibility and simultaneous coverage of several bands in the optical/UV range and in the X-rays, eliminates all possible ambiguities associated with weather conditions and lack of coordination in the different energy bands. In principle, true contemporaneous observations in several energy bands should make it possible to test whether the diverse temporal behavior observed in different objects is related to some fundamental properties of the central engine. More specifically, different combinations of black hole mass  $M_{\text{BH}}$  and accretion rate  $\dot{m}$  may be responsible for the diverse behavior observed in various BH systems. For example, Uttley et al. (2003) hypothesized that objects with large  $M_{\text{BH}}$  and low  $\dot{m}$  should yield a relatively tight X-ray/optical correlation, since they have cooler disks and hence the optical region closer (in units of gravitational radii) to the X-ray emitting central corona. Conversely, for AGN with small  $M_{\text{BH}}$  and high  $\dot{m}$ , the region producing the optical is relatively distant from the X-ray region (the corona) and hence an uncorrelated optical/X-ray behavior may be expected.

In our previous work, we investigated with *SWIFT* the long-term behavior of PKS 0558–504, an X-ray bright radio-loud Narrow-line Seyfert 1 (NLS1) with  $M_{\text{BH}} \sim 3 \times 10^8 M_{\odot}$  likely accreting at super-Eddington rate. The main findings of our 1.5 year monitoring campaign can be summarized as follows. PKS 0558–504 is highly variable at all wavelengths probed by *SWIFT*, with variability levels decreasing from the X-rays to the optical bands. The large-amplitude variations measured by the UVW2 filter are strongly correlated with all the other optical and UV bands and weakly (but significantly) correlated with the X-ray variations. These results, combined with suggestive evidence that in PKS 0558–504 perturbations propagate from the outer to the inner parts of the accretion flow and to the corona, confirm the existence of physical link between disk and corona and disfavor the reprocessing scenario (for more details see Gliozzi et al. (2013)).

Here, to further investigate the link between accretion disk and corona and its putative dependence on  $M_{\text{BH}}$  and  $\dot{m}$ , we study the correlated variability properties of the prototypical bare Seyfert 1 galaxy Ark 120, which has a relatively large black hole mass,  $M_{\text{BH}} \sim 1.5 \times 10^8 M_{\odot}$  (Peterson et al. 2004) and low accretion rate  $L_{\text{bol}}/L_{\text{Edd}} \sim 0.05$  (Vasudevan & Fabian 2007). Past studies have shown that Ark 120 stands out among bright Seyfert galaxies for the lack of any evidence for reddening in IR and UV observations (Ward, et al. 1987; Crenshaw et al. 1999) and warm absorbers (Vaughan et al. 2004) and is highly variable source over the entire spectrum (e.g., Kaspi et al. 2000; Carini et al. 2003; Doroshenko et al. 2008), making it an ideal target for a *SWIFT* monitoring campaign.

This paper is structured as follows. In Section 2, we describe the observations and data reduction. In Section 3 we study the temporal and spectral variability properties with model-independent tools, in Section 4 we describe the re-

sults of a standard spectral analysis, whereas in Section 5 we carry out an inter-band correlation analysis. In Section 6 we summarize our main findings and discuss their implications.

Hereafter, we adopt a cosmology with  $H_0 = 71 \text{ km s}^{-1} \text{ Mpc}^{-1}$ ,  $\Omega_{\Lambda} = 0.73$  and  $\Omega_{\text{M}} = 0.27$  (Bennet et al. 2003). With the assumed cosmological parameters, the luminosity distance of Ark 120 is 142 Mpc.

## 2 OBSERVATIONS AND DATA REDUCTION

Ark 120 was observed by *SWIFT* (Gehrels 2004) between 4 September 2014 and 9 March 2015 with a cadence of one pointing every two days. This observing strategy was devised to preserve the UVOT filter wheel by using the filters of the day U and UVM2, which regularly alternate every two days. The filters choice is based on the fact that U is the “reddest” among standard filters and UVM2 the “bluest” clean filter (UVW2 is slightly bluer than UVM2 with a central wavelength of 1950 Å vs. 2200 Å, but is affected by a red leak). The details of the *SWIFT* monitoring campaign are summarized in Table 1 (dates and exposures) and Table 2 (X-ray count rates and hardness ratios, as well as U and UVM2 fluxes), where only the first four entries are shown for illustrative purposes. The complete tables are available in electronic format. The *SWIFT* XRT (Burrows et al. 2005) observations were performed in windowed timing mode to avoid possible pile-up effects (Hill et al. 2004). For both spectra and light curves, source photons were extracted in a circular region with a radius of 20 pixels (corresponding to  $\sim 47''$ ) centered on the source, and the background was selected using a circle of the same size but shifted along the window, away from the source position. Only single to quadruple events in the energy range of 0.3–10 keV were selected for further analysis. Source and background spectra were extracted from the event file by using XSELECT version 2.3. All the light curves analyzed in Section 3 are background-subtracted. The auxiliary response files were created by the Swift tool `xrtmkarf` and used in combination with the response matrix `swxwt0to2s6psf1.20131212v001.rmf`. We also obtained photometry with the UV/Optical Telescope (UVOT; Poole et al. 2008, Breeveld et al. 2010) in the U and UVM2. Source photons were extracted from a circular region with  $r = 5''$ , and the background from an source-free circular region with a radius of  $20''$ . The UVOT tool `uvotsource` was used to determine the fluxes. The fluxes were corrected for Galactic reddening ( $E_{\text{B}-\text{V}} = 0.113$  obtained from NED) with the standard reddening correction curves by Cardelli et al. (1989). The U and UVM2 images of Ark 120 show point-like sources, suggesting that the galaxy contribution is negligible compared to the AGN emission. Indeed, this conclusion is confirmed by Koss et al. (2011), who studied the properties of the host galaxies of the AGN observed with *SWIFT* BAT and concluded that the galaxy emission of Ark 120 is strongly contaminated by the AGN in all the filters.

**Table 1.** Observation log of Ark 120

Segment	Start time (UT)	End Time (UT)	MJD	Observing time given in s		
				T <sub>XRT</sub>	T <sub>U</sub>	T <sub>UVM2</sub>
01	2014-09-04 01:20:00	2014-09-04 01:36:59	56904.56	992	998	...
02	2014-09-06 04:34:56	2014-09-06 04:51:58	56906.69	1009	...	1000
03	2014-09-08 06:03:36	2014-09-08 06:20:58	56908.75	1026	1019	...
04	2014-09-10 10:50:37	2014-09-10 11:07:58	56910.95	1038	...	1018

**Table 2.** *SWIFT* XRT count rates and HR and UVOT fluxes (mJy) of Ark 120

Segment	XRT rate	XRT HR	U	UVM2
01	1.19±0.03	0.20±0.02	6.93±0.15	...
02	1.25±0.04	0.11±0.02	...	3.57±0.08
03	1.13±0.03	0.15±0.02	6.96±0.15	...
04	1.31±0.04	0.18±0.02	...	3.48±0.08

$HR = (h - s)/(h + s)$ , with  $s = 0.3$ – $1$  keV and  $h = 1$ – $10$  keV. The errors given in this table are statistical errors.

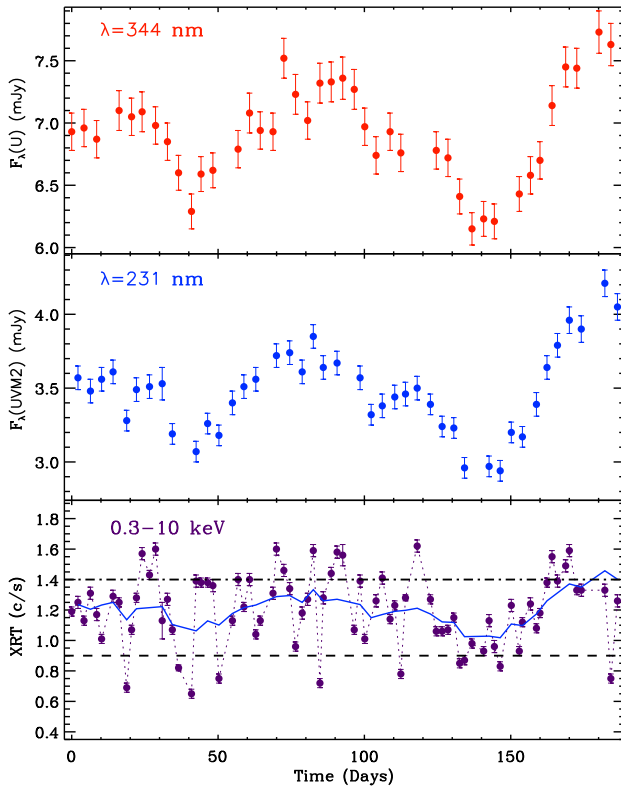


**Figure 1.** *SWIFT* UVOT U (top panel), UVM2 (middle panel) and 0.3–10 keV XRT (bottom panel) light curves of Ark 120 from 4 September 2014 to 9 March 2015. The UV fluxes are corrected for Galactic absorption and expressed in units of mJy. On top of the X-ray time series we superimposed the UVM2 light curve normalized to have the same mean as the X-ray light curve. The dot-dashed and dashed lines on the X-ray light curve represent the threshold values used for the flux-selected spectral analysis.

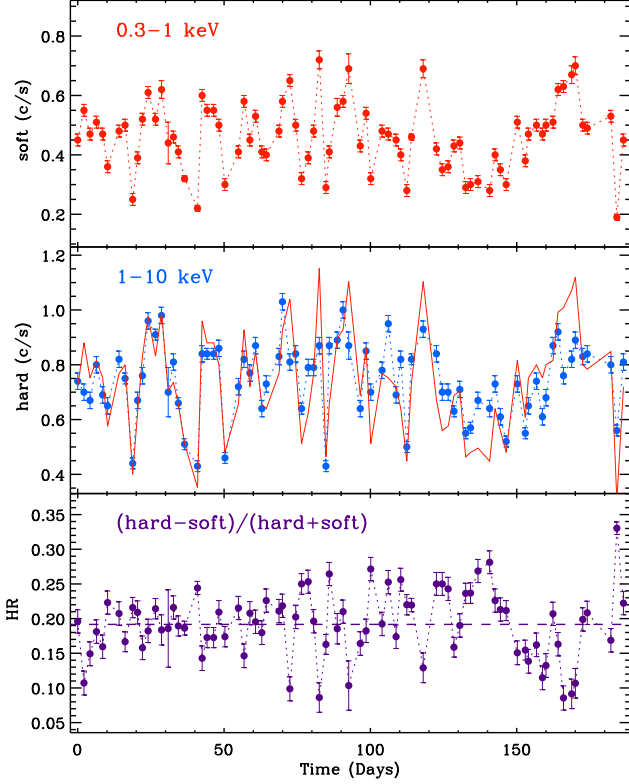
### 3. VARIABILITY ANALYSIS OF Ark 120

Figure 1 shows the UVOT U ( $\lambda = 344$  nm; top panel), UVM2 ( $\lambda = 231$  nm; middle panel) light curves, as well as the 0.3–10 keV XRT light curve (bottom panel) of Ark 120. On top of the X-ray time series we superimposed the normalized UVM2 light curve (blue continuous line) to highlight the similarities and differences between the temporal behavior in the UV and X-rays. While the overall trend seems to be broadly consistent, the X-ray light curve exhibits short-term variability, which is not present in the smoother UV light curves. The dot-dashed and dashed lines on the X-ray light curve represent the threshold values used for the flux-selected spectral analysis (see Section 4); data points above the dot-dashed line have been selected for the “high-flux” spectrum, whereas those below the dashed line define the “low-flux” spectrum.

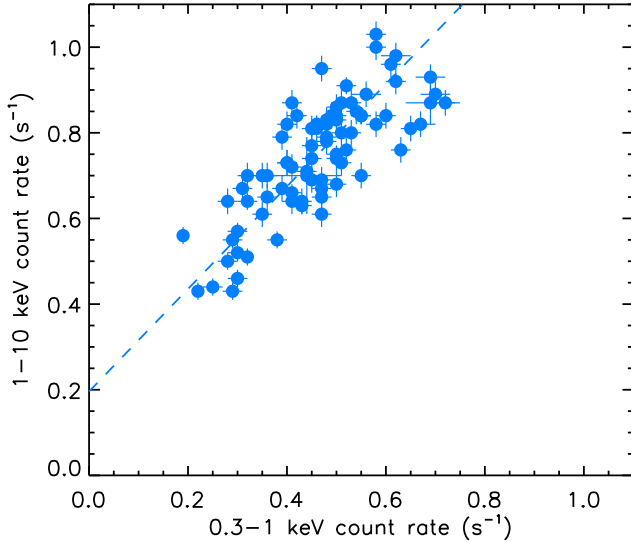
As suggested by the visual inspection of this figure, Ark 120 is highly variable at all wavelengths probed by *SWIFT*. According to a  $\chi^2$  test, the light curves show significant variability with  $\chi^2/dof$  values of 270.5/40, 562.6/41, and 4283.8/80 for the U, UVM2 UVOT filters, and XRT, respectively. An analysis of the fractional variability  $F_{var} = \sqrt{\sigma^2 - \Delta^2}/\langle r \rangle$  (where  $\sigma^2$  is the variance,  $\Delta^2$  the mean square value of the uncertainty associated with each individual count rate, and  $\langle r \rangle$  the unweighted mean count rate) confirms these results, suggesting the presence of a positive trend between variability and energy band:  $F_{var,U} = (5.2 \pm 0.4)\%$ ,  $F_{var,UVM2} = (7.9 \pm 0.4)\%$ ,  $F_{var,XRT} = (19.6 \pm 0.3)\%$ .

Figure 2 shows the soft (0.3–1 keV), hard (1–10 keV), and hardness ratio  $HR = (h - s)/(h + s)$  light curves of Ark 120. To guide the eye, we have superimposed the normalized soft X-ray light curve (red continuous line in the middle panel) on top of the hard X-ray light curve. The similar trend between the two X-ray bands indicates that soft and hard time series vary significantly and nearly in concert. According to a  $\chi^2$  test and fractional variability analysis, the count rate variation are highly significant with  $\chi^2/dof = 2693.5/80$ ,  $F_{var,soft} = (24.9 \pm 0.5)\%$ , and 4283.8/80,  $F_{var,hard} = (17.9 \pm 0.4)\%$  for the soft and hard band respectively. Based on the same tests, the variability of the  $HR$  light curve appears to be statistically significant with  $\chi^2/dof = 801.3/80$  and  $F_{var,HR} = (23 \pm 1)\%$ , suggesting the presence of X-ray spectral variability.

A simple model-independent method to test for spectral variability makes use of the plot of the X-ray hard count rate versus the soft count rate (e.g., Churazov et al. 2001), which is shown in Fig. 3. As expected from the visual inspection of the X-ray light curves, the plot of hard vs. soft count rates shows a strong linear correlation: – the Spearman’s rank correlation coefficient is  $\rho = 0.79$  and associated probability of random correlation  $P_\rho = 1.4 \times 10^{-18}$  –



**Figure 2.** Soft, hard, and hardness ratio,  $HR=(h-s)/(h+s)$  light curves Ark 120. The solid line superimposed on the middle panel represents the normalized soft X-ray light curve. The dashed line in the bottom panel describes the average value of the hardness ratio.



**Figure 3.** Hard vs. soft X-ray count rate plot of Ark 120 obtained in the *SWIFT* XRT campaign. The dashed line represents the best-fit linear model  $Count\ Rate_{1-10\text{keV}} = 0.20 \pm 0.02 + (1.10 \pm 0.04)Count\ Rate_{0.3-1\text{keV}}$ .

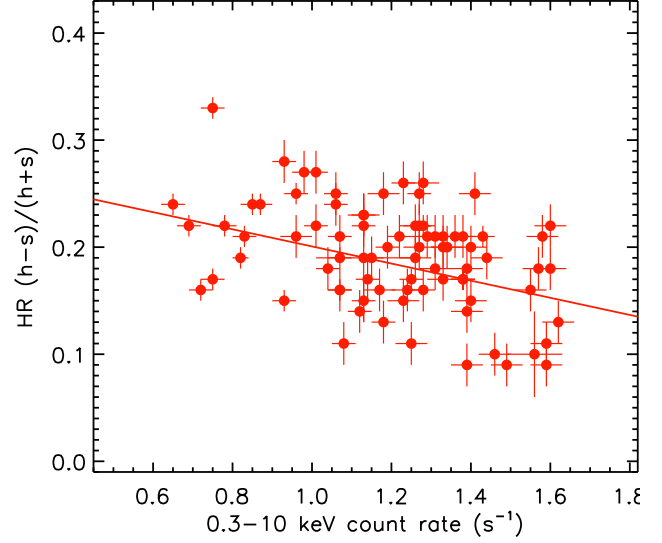


**Figure 4.** Hardness ratio  $HR=(h-s)/(h+s)$  vs. 0.3–10 keV X-ray count rate plot of Ark 120 obtained in the *SWIFT* XRT campaign. The continuous line represents the best-fit linear model  $HR = 0.287 \pm 0.008 - (0.080 \pm 0.007)Count\ Rate_{0.3-10\text{keV}}$ .

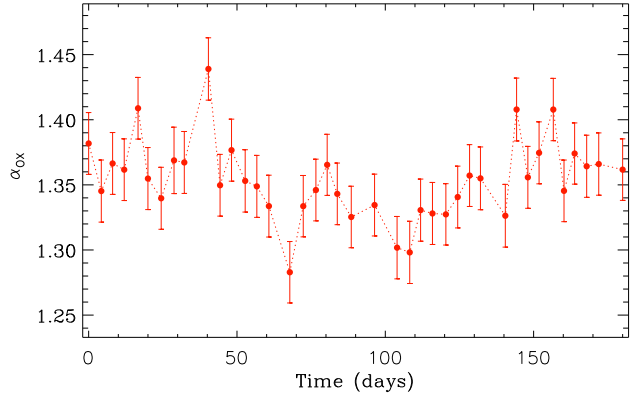


**Figure 5.** Light curve of the broadband spectral index  $\alpha_{OX}$ .

and is well described by the equation  $Count\ Rate_{1-10\text{keV}} = 0.20 \pm 0.02 + (1.10 \pm 0.04)Count\ Rate_{0.3-1\text{keV}}$ , obtained with the routine *fitexy* (Press et al. 1997), which accounts for the errors on both  $y$  and  $x$  axes, and will be adopted in the rest of the paper for any linear correlation analysis. Interestingly, while the slope is roughly consistent with the unity, the positive intercept, inconsistent with zero, suggests the existence of a non-variable hard component.

An additional direct way to study the X-ray spectral variability of AGN is to plot the hardness ratio versus the total flux. The result of this analysis for Ark 120 is shown in Fig. 4, which, despite the substantial scatter, reveals the existence of a shallow but robust anti-correlation ( $\rho = -0.38$ ,  $P_\rho = 5 \times 10^{-4}$ ) described by  $HR = 0.287 \pm 0.008 - (0.080 \pm 0.007)Count\ Rate_{0.3-10\text{keV}}$ , which indicates that the spectrum softens as the source brightens.

Finally, model-independent information about the broadband spectral variability can be inferred by study-

ing the temporal evolution of the broadband spectral index  $\alpha_{\text{OX}} = \log(l_{2500\text{\AA}}/l_{2\text{keV}})/\log(\nu_{2500\text{\AA}}/\nu_{2\text{keV}})$  (Tananbaum et al. 1979). We derived  $\alpha_{\text{OX}}$  from the simultaneous X-ray and UVM2 fluxes, and plotted the light curve in Figure 5, which suggests the presence of a weak variability of the spectral energy distribution (SED):  $\chi^2/dof = 62.6/39$ ,  $F_{\text{var},\alpha_{\text{OX}}} = (1.4 \pm 0.4)\%$ .

In summary, the 6-month *SWIFT* monitoring campaign of Ark 120 confirms the presence of significant large-amplitude variability (for such a large black hole mass) in all bands probed by the UVOT and XRT, with the X-ray band being by far the most variable component, and indicate that the temporal variability of Ark 120 is associated with spectral changes of the X-rays and, to a lesser extent, of the broadband SED.

#### 4 X-RAY SPECTRAL ANALYSIS

The X-ray spectral analysis was performed using the **XSPEC** v.12.9.0 software package (Arnaud 1996). For  $\sim 1$  ks exposure observations, spectra were re-binned within grppha 3.0.0 to have at least 1 photon per bin and fitted with the C-statistic, whereas combined flux-selected spectra were re-binned at 20 counts per channel for the  $\chi^2$  statistic to be valid. The errors on spectral parameters represent the 68% confidence level ( $1-\sigma$ ) for one interesting parameter ( $\Delta\chi^2 = 1$ ). We verified that the two UV data points are well above the extrapolation of the X-ray best-fitting model and are most likely associated with the accretion disk emission. We did not include the UV data in the spectral fitting analysis, because two non-simultaneous data points in the U and UVM2 filters are not sufficient to characterize the properties of the accretion disk.

We carried out a systematic spectral analysis of every observation of the Ark 120 campaign, even though the short exposures of individual *SWIFT* XRT pointings yield X-ray spectra with limited statistics. We adopted a baseline model that comprises two Comptonization components (representing the primary emission produced by the corona and the soft excess) and a Gaussian line to account for the iron  $K\alpha$  line emission. All additive spectral components are absorbed by a column density fixed at the Galactic value  $N_{\text{H}} = 1.01 \times 10^{21} \text{ cm}^{-2}$ , parameterized by the **wabs** model in Xspec. This model choice was guided by the spectral results from past studies with higher signal-to-noise data, and more specifically by a recent study based on long exposures from *XMM-Newton* and *NuSTAR*, that confirmed the presence of a soft-excess, which appears to be consistent with an additional cooler Comptonization component (Matt et al. 2014). At the beginning all parameters are left free to vary. However, given the limited statistics of the spectra, some parameters are poorly constrained and yield unreasonable values when computing their statistical uncertainty; in those cases, the parameters are fixed at their best fit value. The parameters left free during the error calculation are the spectral index and the normalization for the individual observations. For the combined spectra of high- and low-flux cases, more parameters are reasonably defined and therefore can be left free to vary during the error calculations.

Both the soft excess and the coronal emission have been parameterized by the Bulk Motion Comptonization

(BMC) model in Xspec (Titarchuk et al. 1997), which is a simple but comprehensive Comptonization model that can fit both thermal and bulk Comptonization processes, and is described by four parameters:  $kT$  (the temperature of the thermal seed photons),  $\alpha$  (the energy spectral index related to the photon index by the relationship  $\Gamma = 1 + \alpha$ ),  $\log(A)$  (a parameter describing to the Comptonization fraction  $f = A/(1 + A)$ ), and the normalization. We used the BMC model instead of the phenomenological power law model because the BMC parameters are computed in a self-consistent way, and the power law produced by BMC does not extend to arbitrarily low energies.

For illustrative purposes of individual XRT spectra yielded during the Ark 120 campaign, the unfolded spectrum (**eeufspec** in Xspec) and the data-to-model ratio from obsid 34 with net exposure of 1039 s and count rate of  $\sim 1.5$  c/s are shown in Fig. 6. This represents one of the best-case scenarios, since it refers to an observation with relatively long exposure and high count rate. Larger uncertainties are associated to observations with shorter exposures or lower count rates.

All individual observations are reasonably well fitted with this baseline model ( $\chi^2_{\text{red}}$  ranges from 0.6 to 1.14), although only a few spectra statistically require more than one BMC component, suggesting that the model over-parametrizes the low signal-to-noise spectra. Not surprisingly, the model parameters are poorly constrained. Nevertheless, since the model-independent analysis suggests the presence of spectral variability throughout the monitoring campaign, we tested whether this finding can be confirmed by constructing a light curve of photon index, describing the primary X-ray emission. The resulting plot, shown in Fig. 7, suggests that the time series of the photon index is consistent with the hypothesis of constancy because of the large uncertainties associated with the  $\Gamma$  values. This is indeed confirmed by a  $\chi^2$  test, which yields  $\chi^2/dof = 52.6/80$  ( $P_{\chi} = 0.99$ ). Note that the same conclusion is reached using a single BMC model or a power law model to fit the continuum.

In an attempt to test whether the spectrum of Ark 120 genuinely steepens when the source brightens, we combined several individual spectra of observations with low count rate (count rate<sub>0.3–10 keV</sub>  $\leq 0.9$  c/s) to produce a “low-flux” spectrum, and similarly several spectra with high count rate (count rate<sub>0.3–10 keV</sub>  $\geq 1.4$  c/s) to obtain a “high-flux” spectrum. The threshold count rate values, shown in the bottom panel of Fig. 1, were arbitrarily chosen to be distinct from the mean count rate ( $1.20 \pm 0.03$  c/s) and to encompass at least ten individual observations each, in order to increase the S/N of the combined spectra.

The resulting low-flux and a high-flux spectra have well separated mean count rates,  $0.77 \pm 0.02$  c/s and  $1.54 \pm 0.02$  c/s, and net exposures of  $\sim 11$  ksec and  $\sim 12$  ksec, respectively. Importantly, they have considerably higher signal-to-noise ratios compared to individual spectra, as demonstrated by the comparison of Figure 8 with Figure 6. This allows a better characterization of the spectral models, even though some parameters (such as the Comptonization fraction, or the Gaussian line parameters) remain poorly constrained.

Restricting the fit to the 2–10 keV range, to avoid complications with the putative soft excess, the high-flux spectrum appears significantly steeper ( $\Gamma = 1.90^{+0.04}_{-0.02}$ ) than the

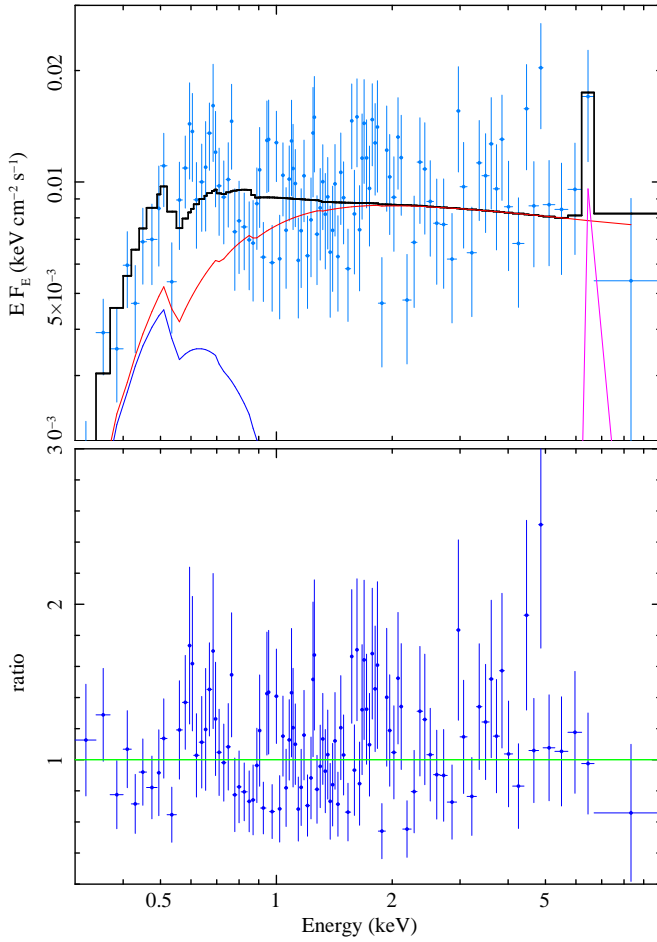


**Figure 6.** Top panel: Unfolded XRT spectrum of Ark 120, obtained using the `eeuvspec` command in Xspec. The model includes two BMC components plus one Gaussian line modified by photo-electric absorption. Bottom panel: data to model ratio.

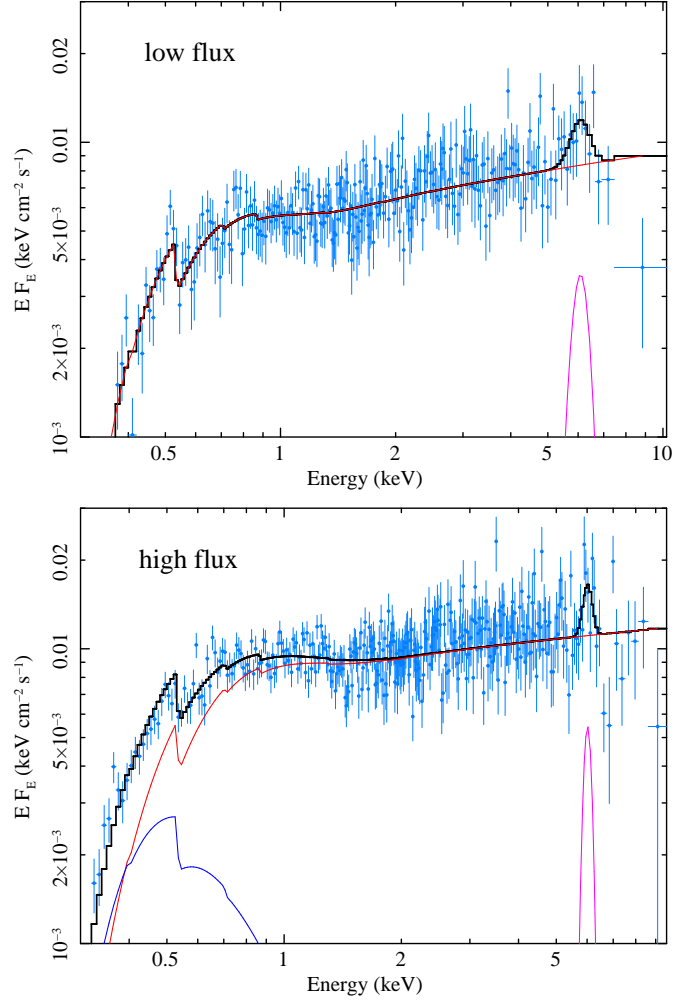


**Figure 8.** Unfolded (`eeuvspec` command in Xspec) XRT spectra of Ark 120 for the combined low-flux and high-flux observations.

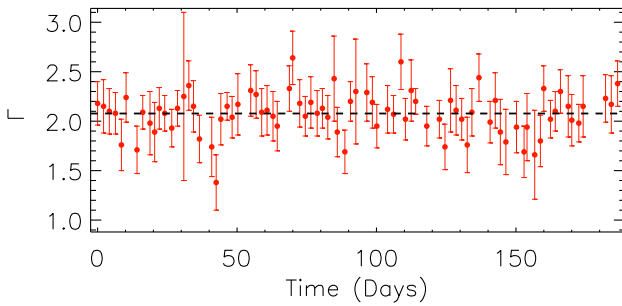


**Figure 7.** Light curve of the X-ray primary emission photon index  $\Gamma$  during the Ark 120 campaign.

low-flux spectrum ( $\Gamma = 1.72^{+0.07}_{-0.06}$ ). The difference in slope between the low- and high-flux spectra is seen in Fig. 8. Note that for unfolded spectra (i.e., plots of  $EF_E$  vs.  $E$ , which are equivalent to the  $\nu f_\nu$  vs.  $\nu$  plots often used in SED studies of AGN), the slope is given by  $2 - \Gamma$ , which means that the steeper positive slope observed in the low-flux unfolded spec-

**Table 3.** Results from the spectral fitting of high- and low-flux of Ark 120

Results	Low-flux	High-flux
$\chi^2/\text{dof}$	1233.5/261	404.6/380
$kT_1$ (keV)	$0.13 \pm 0.01$	$0.15 \pm 0.01$
$\alpha_1$	$0.80 \pm 0.04$	$0.87 \pm 0.04$
$\log(A_1)$	0.08	0.2
$Norm_{BMC1}$	$(2.6 \pm 0.1) \times 10^{-4}$	$(3.5 \pm 0.1) \times 10^{-4}$
$kT_2$ (keV)	...	$0.07 \pm 0.014$
$\alpha_2$	...	4
$\log(A_2)$	...	0.2
$Norm_{BMC2}$	...	$(3.5 \pm 0.1) \times 10^{-4}$
$E_{\text{line}}$ (keV)	$6.3 \pm 0.1$	$6.2 \pm 0.1$
$\sigma_{\text{line}}$ (keV)	0.35	0.1
$Norm_{\text{line}}$	$(8.5 \pm 2.5) \times 10^{-5}$	$(5.2 \pm 2.5) \times 10^{-5}$

The errors given in this table are 1- $\sigma$  errors.

trum (top panel) corresponds to a lower value of  $\Gamma$  compared to the high-flux spectrum (bottom panel).

When the 0.3–10 keV range is considered, both low- and high-flux spectra are reasonably well fitted with a coronal BMC model, and both spectra seem to require a Gaussian line ( $EW \sim 100 - 200$  eV), whose addition reduces the  $\chi^2$  by 5.4 and 6.5 (for three additional parameters) in the low and high-flux cases, respectively. However, only the high-flux spectrum requires a second BMC model to fit the soft energy range. The best-fit values of this fitting procedure are summarized in Table 3.

This is confirmed by the flux-selected spectral fitting analysis that shows that the high-flux spectrum is indeed significantly steeper ( $\Gamma = 1.90^{+0.04}_{-0.02}$ ) than the low-flux spectrum ( $\Gamma = 1.72^{+0.07}_{-0.06}$ ), and that only the high-flux spectrum is statistically improved by the addition of a second BMC model (with  $kT \sim 0.03$  keV) to fit the low-energy part of the spectrum.

In summary, the spectral analysis based on model fitting of flux-selected spectra confirms the existence of spectral variability during the *SWIFT* campaign of Ark 120 revealed by the model-independent spectral variability analysis, with steeper spectra observed when the source has higher count rate.

## 5 CORRELATION ANALYSIS

We used the discrete correlation function (DCF) method of Edelson & Krolik (1988) to compute the correlation function (CCF) at lags  $k = 0, \pm l\Delta t$ , where  $l = 1, \dots, 10$ ,  $\Delta t = 2$  days. As a reference, we used the soft X-ray light curve (hereafter, SX indicates the energy range 0.3–1 keV, and HX the hard X-ray light curve in the 1–10 keV range). We computed the HX vs. SX, M2 vs. SX, U vs. SX, and U vs. M2 cross correlations. In the case of the U vs. M2 correlation, we considered the M2 light curve as reference light curve. Positive lags mean that the reference light curve leads, negative lags indicate that the reference light curve follows. We calculate the centroid of the DCF,  $\tau_{\text{cent}}$ , as the mean of all the DCF points which are  $> 0.75 \times \text{DCF}_{\text{max}}$ , and we accept it as our estimate of the time-lag between two light curves. We also compute the average  $\text{DCF}_{\text{max}}$  as the mean of the DCF values of the same points.

The resulting CCFs are shown in the left panels of Fig. 9. The HX vs. SX shows a strong, narrow peak at zero lag. On the other hand, the UV/X-ray correlations are skewed towards positive lags, suggesting that the SX band variations lead those in the UV band.  $\text{DCF}_{\text{max}}$  values are smaller in the cross-correlations between the UV light curves and the X-ray band. This is not surprising, given the fact that the UV band light curves are much “smoother” than the X-ray band light curves (see Fig. 1). Finally, when U is cross-correlated with the UVM2 band, the CCF is roughly symmetric and shows a strong peak of the order of  $\text{DCF}_{\text{max}} \sim 0.9$ .

In Table 4, we list  $\text{DCF}_{\text{max}}$  together with the time-lags,  $\tau_{\text{cent}}$ , between the various bands along with their respective 90% errors. The errors were estimated using the Monte Carlo simulation method proposed by Peterson et al. (1998). For each light curve pair that we cross-correlated, we produced 10000 simulated light curves following their ran-

dom subset selection prescription. We computed the DCF of each light curve pair,  $\tau_{\text{cent}}$ , and  $\text{DCF}_{\text{max}}$  exactly as we did with the observed light curves. We used the 10000 values to build up the  $\tau_{\text{cent}}$ , and  $\text{DCF}_{\text{max}}$  distribution function. The distribution of the centroid time lags are also plotted in Fig. 9 (right panels). We used these distributions to estimate the 90% confidence limits, which we assume are representative of the 90% confidence limits of the computed  $\tau_{\text{cent}}$  and  $\text{DCF}_{\text{max}}$  values when using the observed light curves.

We do not find a statistically significant detection of delays between any of the light curve pairs considered: all the lags listed in Table 4 are consistent with zero within their 90% confidence limits. In the case of the Hard vs. Soft X-ray, the delays are very small (variations in HX and SX happen almost simultaneously). On the other hand, positive values of  $\tau$  of the order of a few ( $\sim 4$ ) days are tentatively detected in the case of the cross-correlation between the UV light curves and the soft X-ray band. The lags are identical when we consider the cross-correlation between the UVM2 and the U band light curves.

In order to reduce the statistical uncertainty in this cross-correlation analysis and better constrain the delay between X-ray and UV light curves in Ark 120, we tried to combine the U and UVM2 light curves, which have similar trends and do not show any significant delay. To this end, we first interpolated the U light curve, and then shifted the UVM2 light curve by a multiplicative factor obtained by minimizing the RMS between the interpolated U values and the shifted UVM2 values. The resulting combined light curve (hereafter, U+UVM2) is simultaneous to the X-ray light curve and has the same number of data points. The CCF analysis with this combined light curve, shown in Fig. 10, reveals that the soft X-ray light curve leads the UV one by  $7.5 \pm 7$  days (errors indicate the 90% confidence limits). The results are not affected by the uncertainty in the scaling factor when we create the combined U+UVM2 light curve, due to the small uncertainty in the  $F_{\text{var}}$  of the individual light curves.

For completeness, we also performed a cross-correlation between the SX and the X-ray hardness ratio,  $HR$ , and between the combined UV light curve and  $HR$ . In both case, the flux light curves were the reference light curves. The results of this analysis indicate that  $HR$  is anti-correlated with both SX and (U+UVM2).

In summary, our cross correlation analysis confirms that soft and hard X-ray variations are strongly correlated and occur nearly simultaneously. Similarly, the variations in the U and UVM2 filters appears to be correlated and without substantial delay. When the UV light curves are correlated with the X-ray light curve, a possible (but not statistically significant) delay is suggested, with the X-ray leading the variations in the UV bands by a few days. This result is confirmed at a higher significance level when the U and UVM2 are combined and then correlated with the soft X-ray.

## 6 SUMMARY AND CONCLUSION

We first summarize the most relevant results of our *SWIFT* monitoring campaign of Ark 120, and then discuss their implications in the broader context of AGN variability studies.

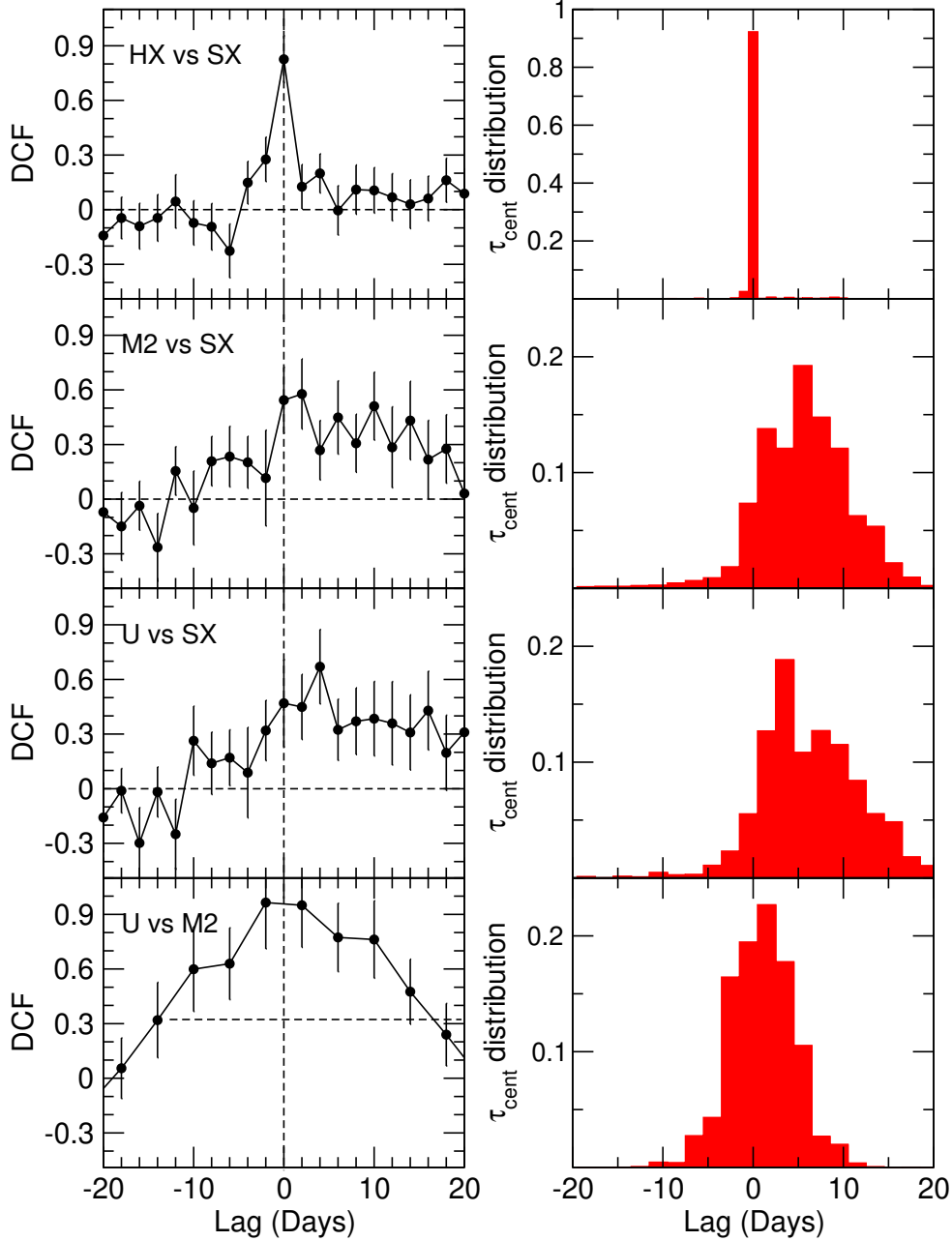


**Figure 9.** *Left panels:* plots of cross-correlation between the 0.3–1 keV soft X-ray flux and the hard (1–10 keV) X-rays (top panel), UVM2 flux (second panel), U flux (third panel), and U vs. UVM2 (bottom panel). *Right panels:* distributions of the centroid time lags for the various cross correlations.

- *Temporal variability:* The 6-month XRT and UVOT monitoring of Ark 120 revealed that strong variability in the X-ray and UV bands, observed in past pointing observations on shorter timescales, occurs on all timescales probed by the *SWIFT* campaign, i.e., from a few days to a few months (see Fig. 1 and Fig. 2). While the X-ray variability is characterized by frequent large-amplitude changes where the count rate can double or halve in periods as short as 2–4 days, the variations observed in the UV bands are smoother with flux changes of the order of 20–40% occurring on timescales of months. This different behavior can be quantified by frac-

tional variability measurements:  $F_{\text{var}}$  increases from  $\sim 5\%$  in the U band, to  $\sim 8\%$  in UVM2, up to  $\sim 20\%$  in the 0.3–10 keV energy band.

- *Spectral variability:* The continuous temporal variability of Ark 120 appears to be associated with persistent spectral variability based on various model-independent analyses. For example, the light curve of the hardness ratio  $HR = (h - s)/(h + s)$  is inconsistent with the hypothesis of constancy at a high confidence level. When  $HR$  is plotted vs. the total X-ray count rate, a weak but statistically significant anti-correlation is found, indicating that the X-ray



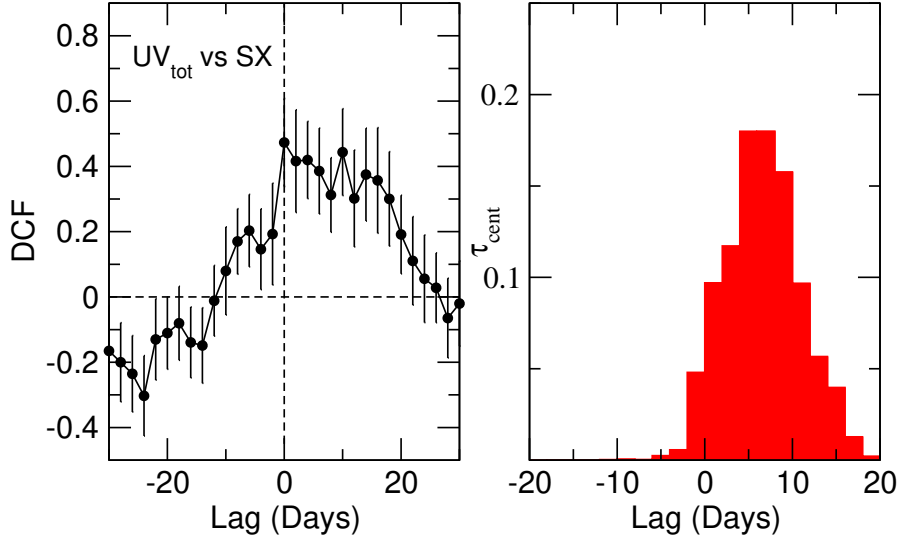


**Figure 10.** *Left panel:* Plots of cross-correlation between the combined (U+UVM2) light curve and the soft X-ray energy band 0.3–1 keV. *Right panel:* distribution of the centroid time lags for this cross correlations.

**Table 4.** UVOT Correlation analysis results

Energy bands (1)	$\tau_{\text{cent}}$ (d) (2)	DCF <sub>max</sub> (3)
HX vs. SX	$0 \pm 0.5$	$0.83^{+0.17}_{-0.13}$
UVM2 vs. SX	$4.5^{+9.5}_{-6.5}$	$0.52^{+0.45}_{-0.02}$
U vs. SX	$4^{+12}_{-5.5}$	$0.67^{+0.30}_{-0.08}$
U vs. UVM2	$4^{+3}_{-8}$	$0.86^{+0.15}_{-0.07}$
(U+UVM2) vs. SX	$7.5 \pm 7$	$0.52^{+0.24}_{-0.12}$
HR vs. SX	$0^{+1}_{-10}$	$-0.79^{+0.26}_{-0.21}$
HR vs. (U+UVM2)	$-15^{+8}_{-6}$	$-0.48^{+0.39}_{-0.08}$

**Columns Table 4:** 1= Correlated light curves. 2= Lags measured in days with the 90% errors. 3= Maximum of DCF with the 90% errors.

spectrum softens when the source brightens, which is the typical behavior observed in Seyfert galaxies (see Fig. 4). Additionally, soft and hard X-ray fluxes are tightly correlated and well described by a linear equation, whose slope is consistent with unity and whose intercept is inconsistent with zero, suggesting the presence of a constant hard component. Finally, the light curve of the broadband spectral index indicates that the entire SED varies throughout the monitoring campaign (see Fig. 5).

• *Spectral analysis:* The spectral analysis of individual  $\leq 1$  ks observations does not provide conclusive results about the long-term spectral variability of Ark 120, due to the limited statistics. However, combining several individual spectra into a low-flux and a high-flux spectrum and then performing a model fitting of these two flux-selected spectra makes it possible to conclude that the steeper-when-brighter behavior is caused by the steepening of the photon index.

• *Correlation analysis:* A cross correlation analysis of the *SWIFT* UVOT and XRT light curves of Ark 120 indicates that soft and hard X-ray variations are strongly correlated and occur nearly simultaneously. Also the U and UVM2 light curves are well correlated with each other and do not show any substantial delay. When the UV light curves are correlated with the X-ray light curve, a possible (but not statistically significant) delay is tentatively detected, with the X-ray leading the variations in the UV bands by a few days (see Fig. 9). This result is confirmed at a higher significance level by using the combined U and UVM2 light curve for the correlation analysis with the soft X-ray light curve (see Fig. 10). Finally, the hardness ratio *HR* appears to be anti-correlated with the soft X-ray light curve, and with the combined UV light curve. While there is no relevant lag between *HR* and X-ray flux, it appears that the changes in the UV light curve are delayed by several days ( $\tau = -15^{+8}_{-6}$  d) with respect to the *HR* changes. The reason for the UV - *HR* correlation was to investigate the possibility that the observed UV photons are the input soft photons up-scattered in the hot corona. In this case, an increase in the flux of soft photons may cause the cooling of the corona, and hence a steepening in the observed X-ray spectrum, as it has been observed in the past (e.g., Nandra et al. 2000). Our results do not support this possibility and may be explained by the fact that the X-rays and *HR* are strongly anti-correlated (with no delay), and the X-rays and UV are moderately correlated with a delay of a few days.

Our study confirms that Ark 120 behaves as a typical Seyfert galaxy with persistent X-ray (and UV) flux variability associated with spectral variability, where the spectrum softens as the source brightens. This spectral behavior too is common to the vast majority of Seyfert galaxies. However, the “bare” nature of Ark 120 ensures that the spectral variability is caused by intrinsic changes in the primary emission, rather than being associated with variations of the absorber surrounding the source, as suggested for many other

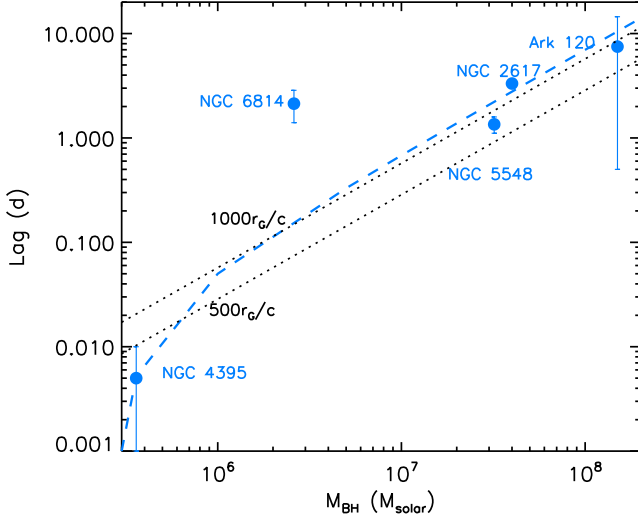


**Figure 11.** Time lags of the UV band with respect to the X-ray band plotted vs. the black hole mass. The dashed line represents the best-fit linear model  $UV/X-ray\ Lag = -0.02 \pm 0.01 + (7.1 \pm 0.4) \times 10^{-8} M_{BH}$ . The dotted dark lines represent the light travel times for  $500 r_G/c$  (bottom) and  $1000 r_G/c$  (top).

AGN. Our results, obtained from a model-independent analysis of monitoring data spanning several months, appear to be consistent with those based on detailed spectral analysis of broadband spectra obtained from the long uninterrupted exposures. For instance, the fact that the intercept of the hard vs. soft X-ray correlation is positive and inconsistent with zero indicates the presence of a constant hard component, which is naturally explained by the reflection component detected by Matt et al. (2014) using high-quality spectra from *XMM-Newton* and *NuSTAR*.

The results from the cross-correlation analysis (the tentative time lag of the UV flux with respect to the X-ray light curve) are consistent with the reprocessing scenario, where changes in the UV/optical emitting accretion disk are driven by changes in the X-ray corona. Although the measured time lag is poorly constrained due to the large statistical uncertainty ( $\tau = 7.5 \pm 7$  d, which is obtained when the combined UV light curve is used for the correlation analysis), to put Ark 120 in context, it is helpful to compare its correlation results with those obtained in similar studies.

In particular, it is interesting to investigate whether there exists a correlation between time lags and  $M_{BH}$  or  $\dot{m}$ , using AGN whose UV and X-ray light curves have been simultaneously monitored by *SWIFT* for several months. In addition to the two objects studied by our group: PKS 0558-504  $-M_{BH} \sim 3 \times 10^8 M_\odot$  and  $\dot{m} \geq 1$  (Gliozzi et al. 2013), and Ark 120  $-M_{BH} = 1.5 \times 10^8 M_\odot$  and  $\dot{m} = 0.005$  (this work), this limited sample of AGN comprises NGC 4395  $-M_{BH} = 3.6 \times 10^5 M_\odot$  and  $\dot{m} = 0.005$  (Cameron et al. 2012), NGC 2617  $-M_{BH} = 4 \times 10^7 M_\odot$  and  $\dot{m} \sim 0.1$  (Shappee et al. 2014), NGC 5548  $-M_{BH} = 3.2 \times 10^7 M_\odot$  and  $\dot{m} = 0.03$  (Edelson et al. 2015), and NGC 6814  $-M_{BH} = 2.6 \times 10^6 M_\odot$  and  $\dot{m} = 0.01$  (Pancoast et al. 2014; Troyer et al. 2016).

In Figure 11 we plotted the time delays between the UV band and the X-ray detected for these objects. For all

objects, we used the lag value reported for the UVOT U filter ( $\lambda_{peak} = 350$  nm), with the exception of NGC 6814 for which only the lag of UVW1 ( $\lambda_{peak} = 260$  nm) was measured. PKS 0558-504 was not included because the detection of a lag was not statistically significant. However, it is worth noting that PKS 0558-504 putative delay ( $\tau = -16.8^{+16.8}_{-14.7}$  days) was of the same order as the one detected in Ark 120, which has a similar black hole mass, but negative (i.e., with the UV emission that appears to lead the X-rays by a few days). It is interesting to note that PKS 0558-504 is the only object for which such a negative delay has been putatively detected and the only AGN of this sample with accretion rate above the Eddington level.

All objects in Fig. 11, with the exception of NGC 6814, are reasonably well fitted with a linear model, represented by the dashed line  $UV/X-ray\ Lag = -0.02 \pm 0.01 + (7.1 \pm 0.4) \times 10^{-8} M_{BH}$ . This finding is qualitatively in agreement with the general picture of black hole systems, where the length-scale is set by the black hole mass, naturally implying a larger physical separation (and hence longer delays) for systems with larger  $M_{BH}$ .

The dotted lines, which represent the light travel times for  $500 r_G/c$  and  $1000 r_G/c$ , suggest that, with the exception of NGC 4395 (for which no significant lag was detected), all AGN of this sample require a physical separation between the X-ray emitting region and the UV region of the order of  $1000 r_G$  or more (NGC 6814). These values are considerably larger than the physical locations of the UV emitting region predicted by the standard accretion disk model; using Equation (2) from Cameron et al. 2012) we obtain values of the order  $100 - 250 r_G$ . We therefore conclude that, for this sample of AGN, these cross-correlation results imply a larger accretion disk compared to the Shakura-Sunyaev standard model, as suggested by recent findings based on micro-lensing studies from Mosquera et al. (2013) and intensive simultaneous monitoring of several energy bands in NGC 5548 (Edelson et al. 2015).

In conclusion, our work indicates that long-term monitoring studies of AGN provide useful information which is complementary to that obtained in long-exposure spectral studies. Importantly, combining Ark 120 correlation results with those of similar studies of AGN monitored by *SWIFT*, suggests the existence of a positive correlation between time lags and black hole mass. Additional monitoring studies of AGN spanning a broader range of  $M_{BH}$  and  $M_\odot$  are necessary to derive a firmer conclusion.

## Acknowledgements

We thank the anonymous referee for the constructive comments that have improved the clarity of the paper. MG acknowledges support by the *SWIFT* Guest Investigator Program under NASA grant NNX15AB64G.

## REFERENCES

- Arévalo, P., Uttley, P., Kaspi, S., Breedt, E., Lira, P., & McHardy, I.M. 2008, MNRAS, 389, 1479
- Arévalo, P., Uttley, P., Breedt, E., Lira, P., McHardy, I.M., & Churazov, E. 2009, MNRAS, 397, 2004
- Arnaud, K. 1996, in ASP Conf. Ser. 101, Astronomical

- Data Analysis Software and Systems V, ed. G. Jacoby & J. Barnes (San Francisco: ASP), 17
- Bennet, C.L. et al. 2003, *ApJS*, 148, 1
- Breedt, E., et al. 2009, *MNRAS*, 394, 427
- Breedt, E., et al. 2010, *MNRAS*, 403, 605
- Breeveld, A.A., et al. 2010, *MNRAS*, 406, 1687
- Burrows, D. et al. 2005, *Space Sci. Rev.*, 120, 165
- Cameron, D.T., et al. 2012, *MNRAS*, 422, 902
- Cardelli, J.A., Clayton, G.C., & Mathis, J.S. 1989, *ApJ*, 345, 245
- Carini, M.T., Noble, J.C., & Miller, H.R. 2003, *AJ*, 125, 1811
- Churazov, E., Gilfanov, M., & Revnivtsev, M. 2001, *MNRAS*, 321, 759
- Crenshaw, D.M., et al. 1999, *ApJ*, 516, 750
- Doroshenko, V.T., Sergeev, S.G., & Pronik, V.I. 2008, *ARep*, 52, 442
- Edelson, R.A. & Krolik, J.H. 1988, *ApJ*, 333, 646
- Edelson, R., et al. 2015, *ApJ*, 806
- Gehrels, N. et al. 2004, *ApJ*, 611, 1005
- Gliozzi M., Papadakis, I.E., Grupe, D., Brinkmann, & W., R  th, C. 2013, *MNRAS*, 433, 1709
- Hill, J.E. et al. 2004, *Proc. SPIE*, 5165, 217
- Kaspi, S., Smith, P.S., Netzer, H., et al. 2000, *ApJ*, 533, 631
- Koss, M., et al. 2011, *ApJ*, 739, 57
- Maoz, D., Edelson, R., & Nandra, K. 2000, *AJ*, 119, 119
- Matt, G., et al. 2014, *MNRAS* 439, 3016
- Mosquera, A.M., et al. 2013, *ApJ*, 769, 53
- Nandra, K., Le, T., George, I.M., Edelson, R.A., Mushotzky, R.F., Peterson, B.M., & Turner, T.J. 2000, *ApJ*, 544, 734
- Pancoast, A., Brewer, B.J., Treu, T., Park, D., Barth, A.J., Bentz, M.C., & Woo, J-H 2014, *MNRAS*, 445, 3073
- Peterson, B.M., Wanders, I., Horne, K., Collier, S., Alexander, T., Kaspi, S., & Maoz, D. 1998, *PASP*, 110, 660
- Peterson, B.M., et al. 2004, *ApJ*, 613, 682
- Poole, T.S. et al. 2008, *MNRAS*, 383, 627
- Press, W.H., Teukolsky, S.A., Vetterling, W.T., & Flannery, B.P. 1997, *Numerical Recipes* (Cambridge: Cambridge Univ. Press)
- Shappee, B.J., et al. 2014, *ApJ*, 788, 48
- Tananbaum, H., Avni, Y., Branduardi, G., et al. 1979, *ApJ*, 234, 9L
- Titarchuk, L., Mastichiadis, A., & Kylafis, N. 1997, *ApJ*, 487, 834
- Troyer, J., et al. 2016, *MNRAS*, 456, 4040
- Uttley, P., Edelson, R., McHardy, I. M., Peterson, B. M., & Markowitz, A. 2003, *ApJ*, 584, L53
- Vaughan, S., Fabian, A.C., Ballantyne, D.R., De Rosa, A., Piro, L., & Matt, G. 2004, *MNRAS*, 351, 193
- Vasudevan, R.V. & Fabian, A.C. 2007, *MNRAS*, 381, 1235
- Ward, M., Elvis, M., Fabbiano, G., Carleton, N.P., Willner, S.P., & Lawrence, A. 1987, *ApJ*, 315, 74